

LETTER TO THE EDITOR

A determination of the LMC dark matter subhalo mass using the MW halo stars in its gravitational wake.

K. J. Fushimi¹, M. E. Mosquera^{1,2}, and M. Dominguez³

¹ Facultad de Ciencias Astronómicas y Geofísicas, University of La Plata. Paseo del Bosque S/N 1900, La Plata, Argentina.
e-mail: kfushimi@fcaglp.unlp.edu.ar

² Dept. of Physics, University of La Plata, c.c. 67 1900, La Plata, Argentina.

³ Instituto de Astronomía Teórica y Experimental, (IATE-CONICET), Observatorio Astronómico de Córdoba, Universidad Nacional de Córdoba, Laprida 854, X5000BGR, Córdoba, Argentina. CONICET, CCT Córdoba

ABSTRACT

Aims. Our goal is to study the gravitational effects caused by the passage of the Large Magellanic Cloud (LMC) in its orbit on the stellar halo of the Milky Way (MW).

Methods. We employed the Gaia Data Release 3 to construct a halo tracers data set consisting of K-Giant stars and RR-Lyrae variables. Additionally, we have compared the data with a theoretical model to estimate the DM subhalo mass.

Results. We have improved the characterisation of the local wake and the collective response due to the LMC orbit. On the other hand, we have estimated for the first time the dark subhalo mass of the Large Magellanic Cloud, of the order of $2 \times 10^{11} M_{\odot}$, comparable to previously reported values in the literature.

Key words. (Galaxies:) Magellanic Clouds– (Cosmology:) dark matter – Galaxy: halo – Galaxies: kinematics and dynamics

1. Introduction

Dark matter (DM) is central to the standard cosmological model (LCDM), providing gravitational support for forming the galaxies and systems of galaxies (Mo et al. 2010). Its existence is backed by a plethora of observational data, including galaxies' rotation curves (Zwicky 1933; Rubin & Ford 1970), strong and weak gravitational lensing effects (Massey et al. 2010; Clowe et al. 2006), and even the presence of the baryonic acoustic oscillation (Planck Collaboration et al. 2020) in the earlier gravitational wells observed in the cosmic microwave background (CMB).

Despite of these successes, we still lack of precise detection in the laboratory (Bernabei et al. 2022; XENON Collaboration et al. 2023; Barberio et al. 2022; Amaré et al. 2022) or by indirect astrophysical observation (Abdalla et al. 2022; Acharyya et al. 2023; Abe et al. 2023). Many theoretical candidates arise beyond the standard model physics models (BSMP), like Weakly Interacting Massive Particles (WIMPs). These massive ($m_{DM} \sim 100$ GeV) particles could weakly interact with nucleons, and therefore signals are looked at by several laboratory and accelerator experiments. Also, its annihilation signals could be detectable through γ -ray emission by high-energy telescopes. Despite a massive experimental effort, DM remains a theoretical hypothesis, albeit one with impressive empirical support.

Other DM candidates could be more massive, such as primordial black holes (PBHs) (Carr & Kühnel 2020) which were recently constrained with a series of consistency tests. Nowadays, there is still room to be an essential contributor to the DM content but limited to small windows in mass (Villanueva-Domingo et al. 2021). Other candidates include massive ultra-

light particles (ULDM) that could reach masses as low as 10^{-23} eV (Hui et al. 2017). Therefore the possible DM mass range remains unconstrained today. Additionally, DM particles could interact with themselves, have or have no spin, and other properties, including their mass, remain elusive.

Depending on the nature of the dark matter particle, there are relevant changes in the structure and number of dark matter haloes and subhalos (Zavala & Frenk 2019). For example, some candidates, like warm dark matter (WDM), introduce a cut-off scale in the initial power spectrum of mass fluctuations ($m_{DM} \sim 1$ KeV), and others a scale during the non-linear evolution phase where the DM particles self-interact (SIDM) (Tulin & Yu 2018). Both processes change the abundance of dark matter subhalos and the density profiles of the DM halos in comparison to the predictions of the CDM model.

Buschmann et al. (2018) showed, using CDM simulations, that the gravitational pull of dark matter subhalos affects the distribution of stars in galactic haloes, and that could be used to discover dark subhalos (those without star formation in situ, a precise prediction of the CDM model) and also allows to test the nature of the DM particles itself. This work simulated a passing dark matter subhalo's perturbation to the phase space stellar distribution. Stars are pulled towards the subhalo as it passes, leaving a distinctive feature in halo stars' velocity and number density known as a wake. This phenomenon was previously analytically described by Weinberg (1986) due to the gravitational friction that provokes the orbital decay of the satellite galaxies that inhabit the DM subhalo.

Garavito-Camargo et al. (2019) using CDM simulations quantified the impact of the LMC's passage on the density and

kinematics of the Milky Way's (MW) DM halo and the observability of these structures in the MW's stellar halo. Their results indicated a pronounced wake, which could be decomposed in a Transient and a Collective response in both the DM and stellar halos distributions. Such effect was observed for the first time in the Milky Way halo stars by Conroy et al. (2021). The authors studied the effects induced by the Magellanic Clouds system merging on selected samples of Milky Way stars with precise Gaia Satellite measurements. This detection, and the increasing availability of stellar data from Gaia DR3 release, paves the way to a more precise measurement of the effect with measurements of the wake on the perturber systems of reference that will allow pursuit testing the DM particle nature using this merger data, as was proposed recently by Foote et al. (2023) (in the context of systems of galaxies see Furlanetto & Loeb (2002); Buehler & Desjacques (2023)). Furthermore, Aguilar-Argüello et al. (2022) and Cunningham et al. (2020) conducted studies on the decomposition into spherical harmonics of both density and velocity, respectively, in order to quantify the response of the dark matter halo to the passage of the Large Magellanic Cloud.

Based on the findings of Conroy et al. (2021), we have used the Gaia Data Release 3 to study the DM subhalo of the Magellanic Clouds and our code developments will allow us to apply the methodology to other MW satellites galaxies and Globular clusters and even to develop methods to detect the presence of the dark subhalos predicted by the CDM model.

This work is organised as follows. In Section 2, we present the data samples selection methodology used to identify the effects of the DM subhalo of the LMC on the MW stellar halo. In Section 3, we briefly describe the theoretical model. Meanwhile, we present our results in Section 4. Section 5 presents the conclusions and future perspectives.

2. Data reduction

We studied the gravitational response of the Milky Way's Halo to the passage of the Large Magellanic Cloud in its orbit. To achieve this, we used the data from the Gaia Data Release 3 (Gaia Collaboration et al. 2022, 2016) and created two catalogues of Halo tracers, namely the K-Giants and RR-Lyraes stars. We followed the steps proposed by Conroy et al. (2021) to address this task.

2.1. K-Giant data set

To construct the K-Giant catalogue, we start the analysis with 21793348 sources characterised by *ruwe* values below 1.4 and parallax measurements from 0.005 up to 0.2 mas. To ensure data quality, we performed a series of cleaning procedures. First, we eliminated sources lacking of proper motion and photometric data. Additionally, we excluded sources with high proper motions and only retained those with $-3 < \mu_\delta < 3$ and $-4 < \mu_{\alpha^*} < 3$. To account for dust extinction, we obtained the dustmap from Green (2018) and considered the SFD map to derive the excess colour, $E(B - V)$. Subsequently, we discarded all sources with $E(B - V) > 0.3$. To obtain the corrected magnitudes, we considered the following coefficients: $A_G/E(B - V) = 2.4$, $A_{BP}/E(B - V) = 2.58$, and $A_{RP}/E(B - V) = 1.65$. To focus solely on the giant branch, we restricted the selection to sources satisfying the condition $1.4 < (BP^* - RP^*) < 2$, where BP^* and RP^* represent the corrected magnitudes. Finally, following Riello et al. (2021), we performed the 3σ cut upon the corrected BP and RP flux excess factor (C^*). After completing the data-cleaning process, we obtained a data set

of 1629851 sources. Among them, only 108795 had measured radial velocity from Gaia. To estimate the radial velocity for the remaining sources, we employed a machine learning algorithm, specifically a RandomForestRegressor (Pedregosa et al. 2011) using the following features: $[ra, dec, pmra, pmdec, phot_g_mean_mag, phot_bp_mean_mag, phot_rp_mean_mag]$. After performing the algorithm, we achieved a score of 0.62 for its evaluation of the test set.

To determine the photometric distance, we used the MIST code (Dotter 2016; Choi et al. 2016; Paxton et al. 2011) to generate an isochrone with the specific LMC's parameters, that are an age of 10 Gyr and metallicity of $[Fe/H] = -1.5$. We restricted the isochrone to an effective temperature from 3800 K to 4400 K, and fitted the polynomial equation

$$M_G = 2.88944(BP^* - RP^*)^2 - 11.9263(BP^* - RP^*) + 8.71506. \quad (1)$$

Afterwards, we implemented several masks to exclude known objects from our analysis. Specifically, we applied angular masks for the Large Magellanic Cloud (LMC), Small Magellanic Cloud (SMC), Sagittarius stream, and satellite dwarf galaxies (Draco, Ursa, Carina, and Sculptor). To preserve as many sources as possible, we considered the distances to the sources in the previous step, except for the SMC, where we removed the entire angular mask. Additionally, we masked the region corresponding to the galactic plane ($|b| < 10^\circ$) and restricted our analysis to objects within a galactic distance range of $30 \text{ kpc} < R_{gal} < 100 \text{ kpc}$.

Following the methodology proposed by Conroy et al. (2021), we employed proper motions to eliminate structures linked to the Sagittarius stream. To achieve this, we initially correct the proper motions due to the solar reflex motion, by the "gala" package (Price-Whelan 2017; Price-Whelan et al. 2020). The used parameters were $R_\odot = 8.122 \text{ kpc}$ (GRAVITY Collaboration et al. 2019), $(V_{R,\odot}, V_{\phi,\odot}, V_{Z,\odot}) = (-12.9, 245.6, 7.78) \text{ km/s}$ (Drimmel & Poggio 2018) and the distance of the Sun from the Galactic mid-plane $Z_\odot = 20.8 \text{ pc}$ (Bennett & Bovy 2019). For $b > 10^\circ$ and $|B_{Sgr}| < 15^\circ$, where B_{Sgr} is the latitude in the frame of Sagittarius orbital plane, we remove part of the northern arm of the stream by taking out the sources that have $\mu_{\alpha^*} > -1.3 \text{ mas/yr}$, $-0.4 < \mu_\delta < 0.3 \text{ mas/yr}$ and $\mu_\delta > 1.7\mu_{\alpha^*} + 0.4$. To eliminate the rest of the north arm, we applied a mask to the region with coordinates $b > 0^\circ$ and $180^\circ < l < 210^\circ$. The final selection of sources is based on proper motions, that is keeping only those that satisfy $\mu_{\alpha^*}^2 + (\mu_\delta + 0.1)^2 < 0.5^2$ (Conroy et al. 2021). By implementing this criterion, one effectively excludes disk stars, stars belonging to the Large and Small Magellanic Clouds, the Sagittarius dwarf spheroidal, and other Sagittarius arms. To ensure the purity of our catalogue specifically for K-Giant stars, we performed a cross-match with the spectral types provided by Gaia (gaiadr3.astrophysical parameters). After this matching, our final data set of K-Giant has 2983 sources.

2.2. RR-Lyrae data set

To build the Halo RR-Lyraes catalogue, we started the process by using the 271779 sources catalogued as RR-Lyraes variables by Gaia. Initially, we performed data cleaning by keeping sources with *ruwe* < 1.4, and excluded the ones that lacked of metallicity. These cuts yielded a set of 129515 sources, out of which only 3584 had radial velocity measurements provided by Gaia. To obtain the radial velocity for the remaining sources, we employed the same machine-learning algorithm previously used for K-Giant stars, and achieved a test set score of 0.47. Similar to the

K-Giant approach, we eliminated all sources with $E(B-V) > 0.3$ and corrected the magnitudes. The absolute magnitude is connected to the metallicity through $M_G = 0.32[\text{Fe}/\text{H}] + 1.11$ (Muraeva et al. 2018), therefore, one can obtain their distances using the distance modulus relationship.

To ensure consistency, we followed a similar approach used with the K-Giant. To eliminate known objects such as LMC, SMC, and dwarf galaxies, we applied an angular mask taking into account the distance to the sources. Additionally, to exclude the Sagittarius stream from our analysis, we employed the cut-off criterion of $|B_{\text{Sgr}}| < 15^\circ$ for $b > 0^\circ$. Then, we excluded the region corresponding to the galactic plane ($|b| < 10^\circ$), and focused our analysis on objects with galactic distances between $30 \text{ kpc} < R_{\text{gal}} < 100 \text{ kpc}$. In the final step, we removed stars that did not satisfy the condition $\mu_{\alpha^*}^2 + (\mu_\delta + 0.1)^2 < 0.5^2$ (Conroy et al. 2021) after performing the solar reflex motion correction to the proper motions. It has been removed 21 sources identified with NCG7006, therefore, the final sample has 2555 sources.

Since our aim is to extract the mass of the dark matter subhalo surrounding the Large and Small Magellanic Cloud, we have performed a transformation of coordinates to a new reference system. This particular coordinate reference system is centred in the centre of mass of the Magellanic Clouds, with the x-axis aligned with the direction of the velocity of the centre of mass (see appendix A for details), and it is considered a rest frame. In order to obtain the position and velocity of the centre of mass we have considered that the LMC mass is nine times the SMC mass (Craig et al. 2021).

3. Theoretical model and Likelihood analysis

We used the theoretical model for stellar wakes from dark matter subhalos proposed by Buschmann et al. (2018), where the authors assumed a Plummer sphere for the density profile of the DM subhalo. From the collisionless Boltzmann equation, they derived the time-independent phase-space distribution function in the subhalo rest frame

$$f(\bar{r}, \bar{v}) = \frac{n_0 e^{-(\bar{v} + \bar{v}_s)^2 / v_0^2}}{\pi^{3/2} v_0^3} \left(1 + \frac{2GM_s}{v_0^2} (\bar{v} + \bar{v}_s) \cdot \bar{\alpha} \right), \quad (2)$$

$$\bar{\alpha} = \frac{1}{rv \sqrt{1 + \frac{R_s^2}{r^2}}} \frac{\sqrt{1 + \frac{R_s^2}{r^2}} \frac{\bar{v}}{v} - \frac{\bar{r}}{r}}{\sqrt{1 + \frac{R_s^2}{r^2}} \frac{\bar{v} \cdot \bar{r}}{rv}}.$$

In the equations, $v_0 = \sqrt{2}\sigma_v$ where σ_v is the velocity dispersion, \bar{v}_s and M_s are the DM subhalo velocity and mass respectively, $R_s = 1.62 \sqrt{M_s / (10^8 M_\odot)}$ and n_0 is the star density inside the region of interest. This expression can be easily extended for three different velocity dispersion by including v_{0x} (σ_{v_x}), v_{0y} (σ_{v_y}) and v_{0z} (σ_{v_z}). In this case, the distribution function in the subhalo rest frame can be written as

$$f(\bar{r}, \bar{v}) = \frac{n_0 e^{-\left(\frac{v_x - v_{sx}}{v_{0x}}\right)^2 - \left(\frac{v_y - v_{sy}}{v_{0y}}\right)^2 - \left(\frac{v_z - v_{sz}}{v_{0z}}\right)^2}}{\pi^{3/2} v_{0x} v_{0y} v_{0z}} (1 + 2GM_s \beta), \quad (3)$$

$$\beta = \left(\frac{v_x - v_{sx}}{v_{0x}^2} \hat{i} + \frac{v_y - v_{sy}}{v_{0y}^2} \hat{j} + \frac{v_z - v_{sz}}{v_{0z}^2} \hat{k} \right) \cdot \bar{\alpha}.$$

In order to obtain the mass of the DM subhalo of the MCS, we have performed a statistical analysis using the likelihood function to compare the reduced observational data and the theoretical model. This analysis was performed by using only the

space data (3D) and the phase-space data (6D). The un-binned likelihood function for the 6D analysis is (Buschmann et al. 2018)

$$p_{6D}(M_s, \theta) = e^{-N_s(M_s)} \prod_{k=1}^{N_d} f(\bar{r}_k, \bar{v}_k), \quad (4)$$

where N_d is the number of stars in the region of interest (sphere of radius R centred in the centre of mass of the MCS) and N_s is the predicted number of stars in the same region. For the Plummer sphere and for the distribution function of Eq. (2), this number can be computed as (Buschmann et al. 2018)

$$N_s(M_s) = \frac{4}{3} \pi R^3 n_0 + \frac{4GM_s n_0}{v_0 v_s} \gamma F\left(\frac{v_s}{v_0}\right),$$

$$\gamma = R^2 \sqrt{1 + \frac{R_s^2}{R^2}} - R_s^2 \text{arcsinh}\left(\frac{R}{R_s}\right),$$

$$F(x) = e^{-x^2} \int_0^x e^{y^2} dy.$$

For the Plummer sphere and for the distribution function of Eq. (3), the predicted number of stars is

$$N_s(M_s) = \frac{4}{3} \pi R^3 n_0 + \frac{4GM_s n_0}{v_{0x} v_{0y} v_{0z}} \gamma I(\bar{v}_0, v_s),$$

$$I(\bar{v}_0, v_s) = \int \frac{d^3 p}{2\pi} e^{-p^2} \cos\left(\frac{2v_s p_x}{v_{0x}}\right) \left(\left(\frac{p_x}{v_{0x}}\right)^2 + \left(\frac{p_y}{v_{0y}}\right)^2 + \left(\frac{p_z}{v_{0z}}\right)^2 \right)^{-1/2}.$$

For the 3D data, the un-binned likelihood function is

$$p_{3D}(M_s, \theta) = e^{-N_s(M_s)} \prod_{k=1}^{N_d} \int d^3 v f(\bar{r}_k, \bar{v}). \quad (5)$$

The same procedure can be used to obtain the distribution function and the predicted number of stars, using a different density profile, for example NFW (Navarro et al. 1997). However, the change in the density profile does not yield analytical solutions, but it can be computed numerically. The results for both density profiles are described in the next section.

4. Results

In Fig. 1, we present a Mollweide projection map displaying the distribution of our final data set of 5538 stars in galactic coordinates (2983 K-Giants and 2555 RR-Lyraes). To enhance the visual representation, the map has been smoothed using Gaussian functions with a full width at half-maximum (FWHM) of 30° . The colour bar represents the density contrast, indicating relative density variation from its mean value across the sample. The past orbit of the LMC is shown with a green line.

The dark blue region corresponds to the masked region representing the galactic plane. It can be observed, two distinct regions of overdensities. The first one, located in the northern hemisphere, with a longitude range between 225° and 315° , is associated with the collective response. On the other hand, the southern feature appears to cover a larger area ($-30^\circ < l < 130^\circ$) and exhibits significant prominence at a longitude of 51° and a latitude of -27° approximated. This overdensity is associated with the local wake. A more minor component is also present in the northern hemisphere, within a longitude range of 30° to 90° . It appears separate from the southern component due to the

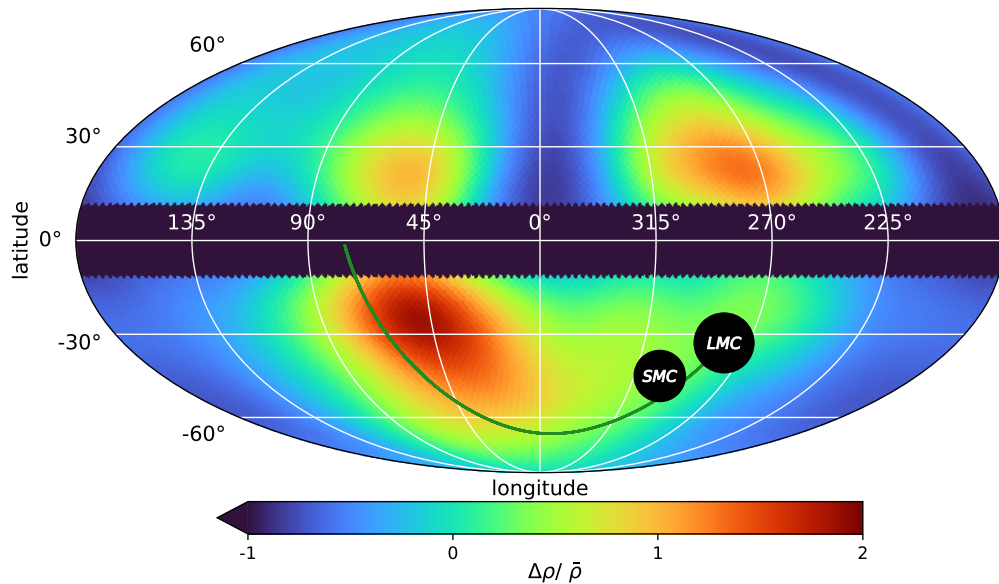


Fig. 1. Density distribution of K-Giant and RR-Lyrae variables (mollweide projection map). The data is smoothed using a Full-Width at Half Maximum (FWHM) of 30°. The green line represents the past orbit of the LMC.

masking of the galactic plane, implemented to prevent contamination. The intensity of the wake is greater than the one of the collective response. The ratio between the counts per pixel of the wake at $l = 51^\circ$, $b = -27^\circ$ and the counts per pixel of the collective response at $l = 277^\circ$, $b = 23^\circ$ (coordinates of the highest overdensity of the collective response) is 1.40 considering the complete data set. This may indicate that the Magellanic Clouds are in their first passage around the Milky Way. As one can see, the LMC past orbit is located over the local wake, and the deviations could be signalling the effect of the DM mass of the wake according to the results of Foote et al. (2023).

Comparing our results with the ones obtained by Conroy et al. (2021), we observe some slight differences in the locations of the overdensities. Specifically, our sample's maximum southern overdensity is slightly displaced further north. Similarly, the maximum northern overdensity in our sample is slightly shifted towards the south and east. In particular, we have compared only our K-Giant sample results with the final public catalogue developed by Conroy et al. (2021), the coordinates of the maximum overdensities of the local wake and the collective response for our data set are ($l = 54^\circ$, $b = -25^\circ$) and ($l = 276^\circ$, $b = 22^\circ$) respectively, meanwhile for Conroy's data are approximated ($l = 49^\circ$, $b = -54^\circ$) and ($l = 326^\circ$, $b = 54^\circ$). Our definition of the local wake is larger than the one proposed by Conroy et al. (2021), and the ratio between the counts per pixel of the wake and the counts per pixel of the collective response at each maximum is 1.25 for our data and 1.33 for Conroy's data-set. However, when we compared our map with the simulations presented in Conroy et al. (2021), we observed quite an agreement regarding the positions of the overdensities.

Fig. 2 presents a 3D plot of our final sample in a system whose origin is the centre of mass of the LMC and SMC (represented with "CM"). The green line represents the past orbit of the LMC. The green sphere represents the sphere that contains the 35% of the LMC Halo mass obtained in this work ($M_s = 2.45 \times 10^{11} M_\odot$), almost all the wake and the collective response are inside of this sphere. According to our previous definitions of wake (pink) and collective response (blue), we ob-

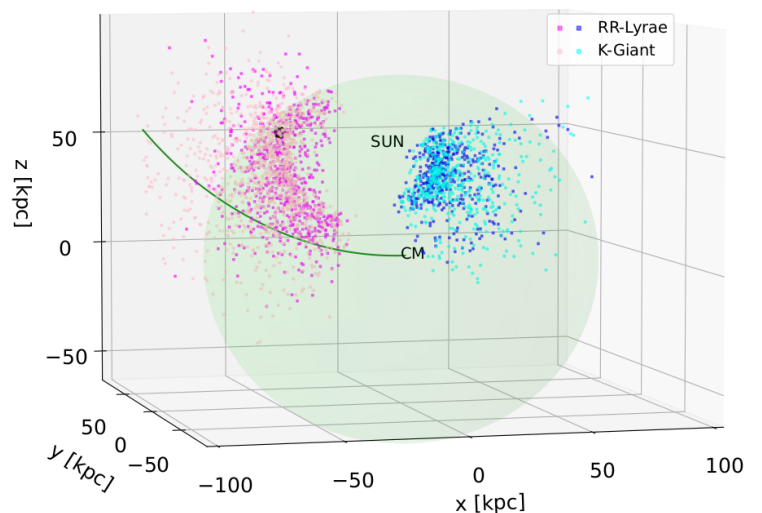


Fig. 2. Wake and Collective Response in the MCS coordinate system with the x-axis aligned towards the direction of the centre of mass velocity. Pink: local wake; blue: collective response. Dots: K-Giants; squares: RR-Lyraes. Black circle: maximum of the wake. CM: centre of mass of LMC and SMC. SUN: position of the Sun in this reference system. Green sphere: sphere that contains the 35% of the LMC Halo mass. Green line: past orbit of the LMC

serve that the wake exclusively exhibits negative values along the x-axis, confirming the prediction that it trails the LMC's orbit (Chandrasekhar 1943; Garavito-Camargo et al. 2019). Furthermore, the collective response is situated in the positive x-axis values. Additionally, we observed that both the RR-Lyrae (squares) and the K-Giant (dots) present the same behaviour. The gaps presented in the figure correspond to the extraction of the galactic plane and the Sagittarius stream.

In Fig. 3, we present the normalised density distribution of the southern wake as a function of position (x , y) within the MC's coordinate system, keeping z fixed in each panel. The dashed grey line traces the historical orbit of the LMC, enabling a visual

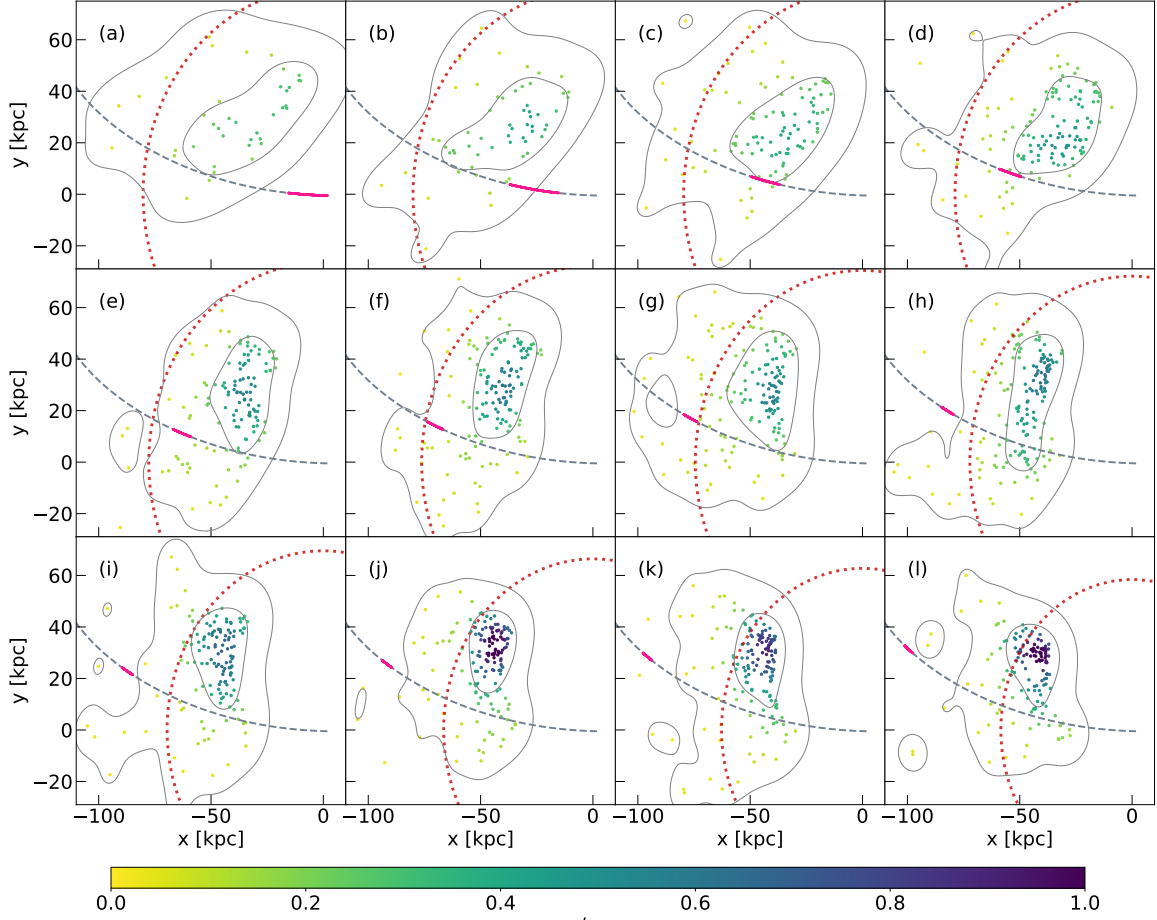


Fig. 3. Normalised superficial density estimation of the south wake (in the MCS coordinate system) at a fixed interval of z , and contour plots (solid grey line). The colour of the points represents the normalised density, as shown in the colour bar. The intervals of z for each panel are defined with a width of 5 kpc and centred at (a) $z = 0$ kpc, (b) $z = 5$ kpc, (c) $z = 10$ kpc, (d) $z = 15$ kpc, (e) $z = 20$ kpc, (f) $z = 25$ kpc, (g) $z = 30$ kpc, (h) $z = 35$ kpc, (i) $z = 40$ kpc, (j) $z = 45$ kpc, (k) $z = 50$ kpc, (l) $z = 55$ kpc. Dotted red line: projection of a sphere of radius R_s in the xy plane. Dashed grey line: the LMC past orbit projection in the xy plane. Pink line: past orbit of the LMC in the correspondent range of z for each panel.

correlation between the wake and the LMC’s trajectory. This relationship becomes particularly evident in panel (j), where the wake exhibits its highest density and aligns with the LMC’s past path, represented by the pink line. Consequently, valuable insights into the LMC’s orbital characteristics could be obtained (Garavito-Camargo et al. 2019). The red dotted line, symbolises the limit of a sphere with a radius of R_s for each panel, corresponding to $M_s = 2.45 \times 10^{11} M_\odot$. This sphere, defined by the Plummer density, encapsulates 35% of the halo’s total mass, and as it has been shown in Fig. 2, most of the wake is located within this sphere. This concentration makes the data set well-suited for estimating subhalo masses. The maximum value of the density is shown in the (j) panel, approximated at $x = -42.9$ kpc, $y = 28.7$ kpc and $z = 53.6$ kpc, where the globular cluster NGC7006 is located. Using the stars in a 8 kpc neighbourhood (206 stars) we computed the velocity dispersion resulting in (43 ± 3) km/s. This velocity dispersion implies a wake mass roughly $6.3 \times 10^{10} M_\odot$ using the relationship reported by Zahid et al. (2018). The wake is a very extended mass distribution and the reported mass should be taken as an approximation. The characterisation of its complete stellar population and dynamical

properties will be addressed in a forthcoming work (Fushimi et al. 2023).

To obtain the DM subhalo mass we maximise the function

$$\lambda_x(M_s) = \ln(p_x(M_s, \theta)) - \ln(p_x(10^5 M_\odot, \theta)), \quad (6)$$

where the sub-index x stands for $6D$ or $3D$ (see Eqs. (4) and (5)), and θ represent all the fixed parameters.

The radius for the region of interest was fixed at $R = 100$ kpc, the subhalo velocity v_s was fixed at 278.49 km/s (van der Marel et al. 2002; Martínez-Delgado et al. 2019) and n_0 was obtained from the reduced observational data described in the previous section. For the velocity dispersion, we have performed a statistical analysis of the data and obtained the velocity standard deviation in each axis, $\bar{v}_0 = (77.97, 73.61, 78.24)$ km/s. For the analysis using Eq. (2), we have considered the larger component of \bar{v}_0 in the calculations. The standard deviation on the subhalo mass was computed as $\Delta \ln \mathcal{L} = -\frac{1}{2}$, as indicated in Barlow (2005).

We have used the Plummer density profile and, to provide a comparison with a more realistic density profile, an NFW-like density profile (Navarro et al. 1997) with a cut-off radius (R_c).

We have set $R_c = 170$ kpc and a characteristic radius (R_s) at 30 kpc. In Fig. 4 we present DM subhalo mass estimation of the LMC published in the literature (Correa Magnus & Vasiliev 2021; Koposov et al. 2023; Shipp et al. 2021; Vasiliev et al. 2020; Erkal et al. 2019; ?) (first six values) along with our results (last four values). The dark matter subhalo mass was computed by using the phase-space distribution function of Eq.(3) (case (a)), of Eq.(2) (case (b)), the space distribution function (case (c)) and the NFW profile and 3D data (case (d)). Our results are consistent despite the distribution function used in the analysis or the density profile. However, the fit obtained using only the space data is slightly lower than the 6D analysis results. Furthermore, our findings agree within 3σ with the literature (Vasiliev 2023).

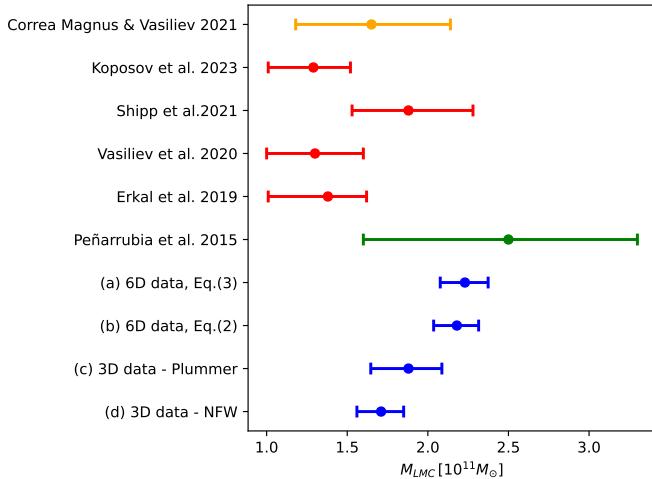


Fig. 4. Dark matter subhalo mass estimation of the LMC. Orange line: kinematic estimation from Milky Way satellites. Red lines: estimation from stellar streams. Green line: estimation based on momentum balance in the Local Group. Blue lines: our results obtained from the likelihood analysis, case (a): 6D data (Eq.(3)), $M_{LMC} = 2.23^{+0.15}_{-0.14} \times 10^{11} M_{\odot}$; case (b): 6D data (Eq.(2)), $M_{LMC} = 2.18^{+0.14}_{-0.13} \times 10^{11} M_{\odot}$; case (c): Plummer profile and 3D data, $M_{LMC} = 1.88^{+0.23}_{-0.21} \times 10^{11} M_{\odot}$; case (d): NFW profile and 3D data, $M_{LMC} = 1.71^{+0.15}_{-0.14} \times 10^{11} M_{\odot}$.

5. Conclusions

In this work, we employed the recently published Gaia Data Release 3 which improves the precision of proper motions. This enabled us to extend the K-Giants catalogue originally provided by Conroy et al. (2021), and also construct a catalogue for RR-Lyrae stars. We reproduced the previously published results and identified the overdensities associated with a wake and the collective response using these two Halo tracers.

Additionally, following Buschmann et al. (2018) theoretical proposal, we were able to estimate for the first time the mass of dark matter subhalo by comparing the observational data and the theoretical model of Buschmann et al. (2018).

We found a reliable estimation of the dark matter halo surrounding the LMC by performing two different analyses, using only the space distribution data and using both, the phase and space data, and two different density profiles for the LMC dark matter halo. Considering a relationship between the Large and Small Magellanic Clouds' mass, our study has successfully determined the mass of the dark matter subhalo of the larger cloud. Even more, our findings are in agreement with prior results (Correa Magnus & Vasiliev 2021; Koposov et al. 2023; Shipp et al.

2021; Vasiliev et al. 2020; Erkal et al. 2019; ?), within 3σ . This consistency with previous studies indicates the reliability of our methodology. Additionally, this method gives competitive errors compared to different mass determination methods.

Acknowledgements. This work was partially supported by grants from the National Research Council of Argentina (CONICET PIP 616). K.J.F. is a Post Doctoral fellow of the CONICET. M.E.M. and M.D. are members of the Scientific Research Career of the CONICET. M.D. work was supported by the Preparing for Astrophysics with LSST Program, funded by the Heising Simons Foundation through grant 2021-2975, and administered by Las Cumbres Observatory.

M.D. thanks valuable suggestions by Nicolás Garavito-Camargo and the support of the CCA and the Flatiron Institute. M.D. also thanks the possibility of virtual participation in the following programs: "Building a physical understanding of galaxy evolution with data-driven astronomy" at the KITP-UCB, the Chicago "Gaia DR3 Sprint" and "Streams22: Community Atlas of Tidal Streams." at the Carnegie Observatories and the Flatiron Institute.

K.J.F. wants to thank Alejo Molina Lera and Martín Gamboa Lerena for the useful discussions.

This work has made use of data from the European Space Agency (ESA) mission *Gaia* (<https://www.cosmos.esa.int/gaia>), processed by the *Gaia* Data Processing and Analysis Consortium (DPAC) <https://www.cosmos.esa.int/web/gaia/dpac/consortium>, and code developed by the *Gaia* Project Scientist Support Team. Funding for the DPAC has been provided by national institutions, in particular, the institutions participating in the *Gaia* Multilateral Agreement.

This research has also made use of the following software: Astropy (Astropy Collaboration et al. 2013), Matplotlib (Hunter 2007), Pandas (McKinney 2010), Seaborn (Waskom 2021), Healpy (Zonca et al. 2019), SciPy (Virtanen et al. 2020), NumPy (Harris et al. 2020), The Jupyter Notebook (Kluyver et al. 2016), and TOPCAT (Taylor 2005).

References

- Abdalla, H., Aharonian, F., Benkhali, F. A., et al. 2022, *Phys. Rev. Lett.*, 129, 111101
- Abe, H., Abe, S., Acciari, V. A., et al. 2023, *Phys. Rev. Lett.*, 130, 061002
- Acharyya, A., Archer, A., Bangale, P., et al. 2023, *ApJ*, 945, 101
- Aguilar-Arquelló, G., Valenzuela, O., & Trelles, A. 2022, *A&A*, 663, A93
- Amaré, J., Cebrián, S., Cintas, D., et al. 2022, *Moscow University Physics Bulletin*, 77, 322
- Astropy Collaboration, Robitaille, T. P., Tollerud, E. J., et al. 2013, *A&A*, 558, A33
- Barberio, E., Baroncelli, T., Bignell, L. J., et al. 2022, *arXiv e-prints*, arXiv:2205.13849
- Barlow, R. 2005, in *PHYSTAT (2005): Statistical Problems in Particle Physics, Astrophysics and Cosmology*, 51–55
- Bennett, M. & Bovy, J. 2019, *MNRAS*, 482, 1417
- Bernabei, R., Belli, P., Bussolotti, A., et al. 2022, in *The Fifteenth Marcel Grossmann Meeting on General Relativity*, Edited by E. S. Battistelli, ed. E. S. Battistelli, R. T. Jantzen, & R. Ruffini, 1285–1290
- Buehler, R. & Desjacques, V. 2023, *Phys. Rev. D*, 107, 023516
- Buschmann, M., Kopp, J., Safdi, B. R., & Wu, C.-L. 2018, *Phys. Rev. Lett.*, 120, 211101
- Carr, B. & Kühnel, F. 2020, *Annual Review of Nuclear and Particle Science*, 70, 355
- Chandrasekhar, S. 1943, *ApJ*, 97, 255
- Choi, J., Dotter, A., Conroy, C., et al. 2016, *ApJ*, 823, 102
- Clowe, D. et al. 2006, *Astrophys. J.*, 648, L109
- Conroy, C., Naidu, R. P., Garavito-Camargo, N., et al. 2021, *Nature*, 592, 534
- Correa Magnus, L. & Vasiliev, E. 2021, *Monthly Notices of the Royal Astronomical Society*, 511, 2610
- Craig, P., Chakrabarti, S., Baum, S., & Lewis, B. T. 2021, *arXiv e-prints*, arXiv:2107.09791
- Cunningham, E. C., Garavito-Camargo, N., Deason, A. J., et al. 2020, *The Astrophysical Journal*, 898, 4
- Dotter, A. 2016, *ApJS*, 222, 8
- Drimmel, R. & Poggio, E. 2018, *Research Notes of the American Astronomical Society*, 2, 210
- Erkal, D., Belokurov, V., Laporte, C. F. P., et al. 2019, *MNRAS*, 487, 2685
- Foote, H. R., Besla, G., Mocz, P., et al. 2023, *arXiv e-prints*, arXiv:2307.00053
- Furlanetto, S. R. & Loeb, A. 2002, *The Astrophysical Journal*, 565, 854
- Fushimi, K. J., Mosquera, M. E., & Dominguez, M. 2023, in preparation
- Gaia Collaboration, Prusti, T., de Bruijne, J. H. J., et al. 2016, *A&A*, 595, A1
- Gaia Collaboration, Vallenari, A., et al. 2022, *arXiv e-prints*, arXiv:2208.00211
- Garavito-Camargo, N., Besla, G., Laporte, C. F. P., et al. 2019, *The Astrophysical Journal*, 884, 51

- GRAVITY Collaboration, Abuter, R., Amorim, A., et al. 2019, *A&A*, 625, L10
- Green, G. 2018, *The Journal of Open Source Software*, 3, 695
- Harris, C. R., Millman, K. J., van der Walt, S. J., et al. 2020, *Nature*, 585, 357
- Hui, L., Ostriker, J. P., Tremaine, S., & Witten, E. 2017, *Phys. Rev. D*, 95, 043541
- Hunter, J. D. 2007, *Computing in Science and Engineering*, 9, 90
- Kluyver, T., Ragan-Kelley, B., Pérez, F., et al. 2016, in *IOS Press*, 87–90
- Koposov, S. E., Erkal, D., Li, T. S., et al. 2023, *Monthly Notices of the Royal Astronomical Society*, 521, 4936
- Martínez-Delgado, D., Vivas, A. K., Grebel, E. K., et al. 2019, *A&A*, 631, A98
- Massey, R., Kitching, T., & Richard, J. 2010, *Reports on Progress in Physics*, 73, 086901
- McKinney, W. 2010, in *Proceedings of the 9th Python in Science Conference*, ed. S. van der Walt & J. Millman, 51 – 56
- Mo, H., van den Bosch, F., & White, S. 2010, *Galaxy Formation and Evolution* (Cambridge University Press)
- Muraveva, T., Delgado, H. E., Clementini, G., Sarro, L. M., & Garofalo, A. 2018, *MNRAS*, 481, 1195
- Navarro, J. F., Frenk, C. S., & White, S. D. M. 1997, *ApJ*, 490, 493
- Paxton, B., Bildsten, L., Dotter, A., et al. 2011, *ApJS*, 192, 3
- Pedregosa, F., Varoquaux, G., Gramfort, A., et al. 2011, *Journal of Machine Learning Research*, 12, 2825
- Planck Collaboration, Aghanim, N., Akrami, Y., et al. 2020, *A&A*, 641, A6
- Price-Whelan, A., Sipőcz, B., Lenz, D., et al. 2020, *adrs/gala: v1.3*
- Price-Whelan, A. M. 2017, *The Journal of Open Source Software*, 2
- Riello, M., De Angeli, F., Evans, D. W., et al. 2021, *A&A*, 649, A3
- Rubin, V. C. & Ford, W. Kent, J. 1970, *Astrophys. J.*, 159, 379
- Shipp, N., Erkal, D., Drlica-Wagner, A., et al. 2021, *The Astrophysical Journal*, 923, 149
- Taylor, M. B. 2005, in *Astronomical Society of the Pacific Conference Series*, Vol. 347, *Astronomical Data Analysis Software and Systems XIV*, ed. P. Shopbell, M. Britton, & R. Ebert, 29
- Tulin, S. & Yu, H.-B. 2018, *Physics Reports*, 730, 1, dark matter self-interactions and small scale structure
- van der Marel, R. P., Alves, D. R., Hardy, E., & Suntzeff, N. B. 2002, *AJ*, 124, 2639
- Vasiliev, E. 2023, *Galaxies*, 11, 59
- Vasiliev, E., Belokurov, V., & Erkal, D. 2020, *Monthly Notices of the Royal Astronomical Society*, 501, 2279
- Villanueva-Domingo, P., Mena, O., & Palomares-Ruiz, S. 2021, *Frontiers in Astronomy and Space Sciences*, 8
- Virtanen, P., Gommers, R., Oliphant, T. E., et al. 2020, *Nature Methods*, 17, 261
- Waskom, M. L. 2021, *Journal of Open Source Software*, 6, 3021
- Weinberg, M. D. 1986, *ApJ*, 300, 93
- XENON Collaboration, Aprile, E., Abe, K., et al. 2023, *arXiv e-prints*, arXiv:2303.14729
- Zahid, H. J., Sohn, J., & Geller, M. J. 2018, *ApJ*, 859, 96
- Zavala, J. & Frenk, C. S. 2019, *Galaxies*, 7
- Zonca, A., Singer, L., Lenz, D., et al. 2019, *The Journal of Open Source Software*, 4, 1298
- Zwicky, F. 1933, *Helv. Phys. Acta*, 6, 110

Appendix A: LMC rest frame

The coordinate system used to compare the data with the theoretical model has its origin in the LMC and SMC centre of mass and the x -axis orientated according to the DM subhalo velocity v_s . In order to obtain the coordinates of our data set in such rest frame, we have performed the following steps

1. we boosted the data to the new frame by $\bar{r}_{boost} = \bar{r}_{obs} - \bar{r}_{cm}$;
2. we performed the rotations upon the boosted data using the matrix

$$M = \begin{pmatrix} \cos \theta_1 \cos \theta_2 & \sin \theta_1 \cos \theta_2 & \sin \theta_2 \\ -\sin \theta_1 & \cos \theta_1 & 0 \\ -\cos \theta_1 \sin \theta_2 & -\sin \theta_1 \sin \theta_2 & \cos \theta_2 \end{pmatrix}, \quad (\text{A.1})$$

to obtain the coordinate (x', y', z') in the new rest frame. The velocity has to be transformed as well and, the final velocity must be boosted in $\bar{v}_s = v_s \hat{i}'$. The angles are defined as

$$\tan \theta_1 = \frac{(v_{cm})_y}{(v_{cm})_x}, \quad (\text{A.2})$$

$$\tan \theta_2 = \frac{(v_{cm})_z}{\sqrt{(v_{cm})_x^2 + (v_{cm})_y^2}}, \quad (\text{A.3})$$

where $((v_{cm})_x, (v_{cm})_y, (v_{cm})_z)$ is the centre of mass velocity in the solar coordinate system.